Feature Extraction Method of Series Arc Fault Occurred in Three-Phase Motor With Inverter Circuit

Hongxin Gao, *Member, IEEE*, Zhiyong Wang, *Member, IEEE*, Congxin Han, Aixia Tang, Fengyi Guo, *Senior Member, IEEE*, and Baifu Li

***Abstract*—Series arc fault is one of the main causes of electrical fire. In a three-phase motor with inverter circuit, it is difficult to accurately identify series arc fault occurred in the lines at the back of the inverter, especially when the power supply contains complicated harmonics. To solve this problem, a new feature extraction method of the series arc fault based on the current signal measured at the front of the inverter (CSMFI) was proposed. The series arc fault experiments under different harmonic power supply conditions were carried out in the three-phase motor with inverter circuit. Five-layer decomposition was performed on the CSMFI by using empirical wavelet transform. The attractor track matrix (ATM) of each decomposed signal was established. The fault features of the series arc fault were obtained by calculating and selecting the singular values of the ATM. The series arc fault was identified by using an optimized support vector machine. The effectiveness of the method and its applicability under different experimental conditions were tested. The method can simultaneously identify the series arc fault occurred in the lines at the front or back of the inverter by analyzing the CSMFI. It also has strong anti-interference ability.**

***Index Terms*—Attractor track matrix, empirical wavelet transform, fault feature extraction, series arc fault, singular value decomposition, support vector machine.**

I. Introduction

In AC power distribution system, due to the influence of mechanical vibration, drag force, extrusion, and harsh environmental conditions, problems such as looseness of electrical connectors, corrosion of contact surfaces, and line extrusion often occur. These problems will increase the contact resistance, and cause glow or spark discharge. In serious case, a series arc fault will occur. The series arc fault is accompanied by a high temperature above 4000°C, which is much higher than the ignition point of combustible materials such as cable insulation. The series arc fault is one of the main causes of electrical fire [1]. In addition, when a series arc fault occurs in the three-phase motor or three-phase motor with inverter circuit, it will cause the power quality problems such as three-phase current unbalance, the increase of harmonic, and so on. In this case, the energy consumption, mechanical vibration, temperature rise, and noise of the three-phase motor will also increase. The fault current of series arc fault is lower than the normal operating current, so the existing overcurrent protection devices cannot detect such fault and realize fault protection. Therefore, it is necessary to further study the detection method of the series arc fault and then develop the arc fault circuit interrupter (AFCI). When the AFCI identifies a series arc fault, it will act in time to power OFF the circuit, so as to effectively avoid the electric fire caused by the series arc fault.

At present, the research on the ac series arc fault is mainly concentrated in civil, aviation, and industrial fields.

In the civil field, the research on the detection method of the series arc fault was conducted for some typical household loads such as an incandescent lamp, vacuum cleaner, electromagnetic furnace, washing machine, electric drill, hair dryer, and so on. Artale *et al.* [2] analyzed the refined frequency spectrum between 0 and 500 Hz of the current signal by using Chirp-Z transform (CZT), and obtained the fault features of the series arc fault by calculating a set of low-frequency indicators. Qu *et al.* [3] proposed a sparse representation method on the basis of the L_p norm with an adjustable regularization order, and realized the detection of the series arc fault by comparing residual and projection coefficient. Lu *et al.* [4] used the wavelet coefficients of current signal to construct a Hank matrix, and the mean, root-mean-square (RMS), and standard deviation of the singular values of the matrix were used as the feature of the series arc fault. Wu and Liu [5] calculated the high-frequency coefficient of the current signal by wavelet transform and used its energy as the fault feature. Wang *et al.* [6] applied the raw current signal as the input features of a convolutional neural network, and developed an ArcNet model to detect the series arc fault. Kim *et al.* [7] used the energy of a band-pass filtered voltage signal as fault features and detected the series arc fault by using threshold method. Jiang *et al.* [8] extracted the time domain, frequency domain, and wavelet packet energy features of the current signal, selected an effective feature combination for different loads by using random forest algorithm, and then identify the series arc fault by using a deep neural network.

Manuscript received December 31, 2021; revised February 27, 2022; accepted March 28, 2022. Date of publication April 1, 2022; date of current version May 23, 2022. This work was supported in part by the National Natural Science Foundation of China under Grant 52077158, in part by the Scientific Research Fund Project of Education Department of Liaoning Province, China under Grant LJ2020QNL020, and in part by Liaoning Revitalization Talents Program under Grant XLYC1802110. Recommended for publication by Associate Editor A. J Marques Cardoso. *(Corresponding author: Fengyi Guo.)*

Hongxin Gao, Zhiyong Wang, Congxin Han, Aixia Tang, and Baifu Li are with the Faulty of Electrical and Control Engineering, Liaoning Technical University, Huludao 125105, China (e-mail: 747829373@qq.com; wangzhiyong@lntu.edu.cn; 471820204@stu.lntu.edu.cn; 471810020@stu.lntu.edu.cn; 1911080503@stu.lntu.edu.cn).

Fengyi Guo is with the College of Electrical and Electronic Engineering, Wenzhou University, Wenzhou 325035, China (e-mail: 20195207@wzu.edu.cn).

Color versions of one or more figures in this article are available at https://doi.org/10.1109/TPEL.2022.3164246.

Digital Object Identifier 10.1109/TPEL.2022.3164246

In the aviation field, the research on the detection method of series arc fault was conducted for resistive load, resistance-inductance load, resistance-capacitance load, transformer, autotransformer rectifier, and so on. Zeng *et al.* [9] analyzed the time domain and frequency domain characteristics of the current signal, and calculated the standard deviation of the RMS of the current, the standard deviation of dc component, and the sum of the odd harmonics. These variables were used as the fault features of the series arc fault. Cui and Tong [10] analyzed the current data using Levene's test and used its significance levels as the feature of the series arc fault. Gao *et al.* [11] conducted integrated empirical mode decomposition of the current signal, selected the energy entropy of the modal components with an obvious difference as the fault feature, and utilized a back propagation neural network optimized by Levenberg–Marquard algorithm to detect the series arc fault. Cui *et al.* [12] conducted time-frequency analysis on the current signal by using generalized S-transform, used the RMS and energy of 2 kHz component as the features of the series arc fault, and applied a support vector machine (SVM) to identify the fault.

In the industrial field, the research on the detection method of series arc fault was conducted for the switchgear, three-phase motor load, and three-phase motor with inverter load. Parikh *et al.* [13] used arc sound and arc light sensors to detect the series arc fault in switchgear. Hussain *et al.* [14] used a differential electric field sensor to measure the electromagnetic signal radiated by the series arc fault in switchgear. The signal was de-noised by using wavelet transform and used as a basis for judging the fault. Wang *et al.* [15] used a R7154 type photomultiplier tube equipped with a filter to measure the ultraviolet power of the arc radiation, and applied a set power threshold to detect the series arc fault in switchgear. Zhang and Ma [16] collected the current and arc light signals, and realized the detection of the series arc fault in switchgear by using expert system evaluation method. Saleh *et al.* [17] extracted the high-frequency components of the current signal by using five exponentially modulated Kaiser window-based high-pass filters, and utilized its phase as the fault feature of the series arc fault. Gao *et al.* [18] constructed an attractor track matrix (ATM) by analyzing the current signal and calculated the singular values of the matrix. The singular values were used as the fault feature. Guo *et al.* [19] constructed a feature matrix of the current signal by S-transform, extracted the singular value of the matrix as fault feature, and used an SVM optimized by genetic algorithm to detect the series arc fault. Guo *et al.* [20] constructed a gray image by using the wavelet packet decomposition of the current differential signal, and obtained the arc fault features by solving the gray-gradient co-occurrence matrix of the gray image. The SVM optimized by a particle swarm optimization algorithm was used to detect the series arc fault. Li *et al.* [21] realized the detection and line selection of the arc fault by using a recurrent neural network, which was trained by directly using three-phase current signals. Gao *et al.* [22] analyzed the change of single-phase current signal from time domain to frequency domain by using fractional Fourier transform, and extracted the fault feature of the series arc fault by using the two-level block singular value decomposition (SVD) method. Han *et al.* [23] used the kurtosis and skewness of the fifth and sixth principal components of two current signals and a voltage signal as the fault features of the series arc fault, and then utilized a firefly algorithm optimized SVM to identify the fault.

The power supply, environmental conditions, and the experimental loads used in [2]–[12] are quite different from those in the industrial field. In [24]–[27], a dc–ac type inverter is used as the experimental load. But the signal type of its current signal is completely different from that of the ac–dc–ac type inverter, which are widely used in the industrial field. So it is difficult to directly apply the research in [2]–[12] and [24]–[27] to the general industrial field.

In [13]–[16], the physical characteristics of arc discharge such as arc light, arc sound, and electromagnetic radiation, and so on are used to detect the series arc fault in switchgear. In this case, sensors must be installed near the location of the fault, so it is difficult to effectively detect the series arc fault at unknown positions in long distribution lines. In [17], it does not mention the applicability of the proposed detection method of the series arc fault to the industrial three-phase motor with inverter load. The inverter is a kind of non-linear load, which will produce lots of harmonic interference during operation. So it is more difficult to detect the series arc fault in the three-phase motor with inverter load than that in the three-phase motor load.

In our previous papers [18]–[23], some detection methods of the series arc fault occurred in industrial three-phase motor with inverter circuit were discussed. These methods still have the following shortcomings.

a) All the proposed methods are assured that the series arc fault occurs in the lines at the front of the inverter (SAFOFI). However, the series arc fault may also occur in the lines at the back of the inverter. How to detect the series arc fault occurred at the back of the inverter (SAFOBI) has not been studied yet.
b) The series arc fault experiments in [18]–[22] are conducted with a commercial power supply in the laboratory. Due to the power quality of the power supply used in the industrial field is usually worse than that of a commercial power supply, the proposed method does not consider whether it is suitable to detect the series arc fault under poor power quality conditions.
c) The feature extraction method of the series arc fault in [22] and [23] requires a large amount of computation.
d) The method proposed in [23] can be used to detect the series arc fault occurred in complicated harmonic circuit. But it needs two current signals and a voltage signal to accurately detect the fault. Three sensors in total are needed to implement the scheme. It is inconvenient to some extent.

For an inverter with ac–dc–ac structure, when a series arc fault occurs at the back of the inverter, it will make the output three-phase current of the inverter unbalance. Since the output power of the inverter is obtained by the transformation of the input three-phase power supply through the internal circuit of the inverter, so the change of the output current signal of the inverter will definitely affect its input current signal through the

above-mentioned conversion circuits. Therefore, when a series arc fault occurs at the back of the inverter, the output current of the inverter will change. It will vary the current at the front of the inverter, and cause the difference of the current between in normal and arc fault state. No matter the series arc fault generated in the lines at the front or back of the inverter, if we can identify it by only analyzing the current signal measured at the front of the inverter (CSMFI), it will save the current transformers installed in the lines at the back of the inverter, reduce the calculation of data analysis, and simplify the system.

To solve the above-mentioned problems, a new fault feature extraction method of the series arc fault based on CSMFI was proposed. The main academic contributions and innovations of this article are as follows.

1) The experiments on SAFOBI under different harmonic power conditions are conducted for the first time, and a new idea to simultaneously detect the SAFOBI and the SAFOFI by analyzing the CSMFI is proposed.
2) A novel fault feature extraction method with filtering ability is proposed by using empirical wavelet transform (EWT), reconstruction of attractor track matrix (RATM), and SVD. It has the advantages of small computation and strong anti-interference ability. The effectiveness of the method is also verified under different testing conditions.

The rest of this article is structured as follows. Section II describes the experimental platform, experimental scheme of the series arc fault, and briefly analyzes the experimental results. Section III introduces the basic theory and realization steps of the feature extraction method in detail. Section IV analyzes the detection performance (i.e., accuracy and operation time) of the proposed method and several existing extraction methods by using an optimized SVM. It also tests the effectiveness of the method under different Gaussian noise interference conditions. Section V verifies the applicability of the method under different loads, inverter's operation parameters, working current, and transient arc faults conditions. Finally, Section VI concludes the article and outlines future research.

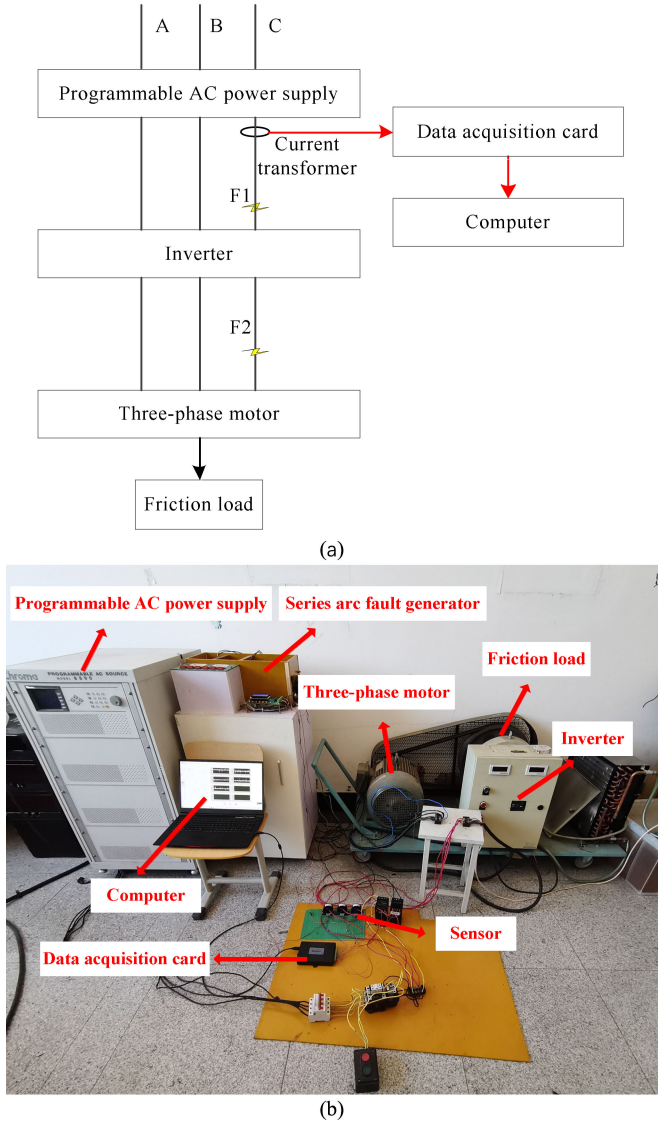

Fig. 1. Experimental platform. (a) Structure. (b) Picture.

II. Series Arc Fault Experiments

A. Experimental Platform

The experimental platform is shown in Fig. 1. A Chroma 6590 type programmable ac power supply was used as the power supply. It can output a three-phase voltage with different harmonic contents. The output voltage is 380 V and its fundamental frequency is 50 Hz. A series circuit consisted of a three-phase asynchronous motor and an inverter was used as the experimental load. Here, a VFD110E43A type inverter was used. Its rated power is 11 kW. Its input voltage is a three-phase voltage, whose RMS is between ac 380 V and ac 480 V and rated frequency is 50 Hz or 60 Hz. And the range of its output frequency is from 0.1 to 600 Hz. An Y160M-6-11 kW type three-phase motor was used. Its rated power is 11 kW. It has six poles, and its rated speed is 970 r/min. The motor adopts delta connection.

The series arc faults experiments under three kinds of working state conditions were carried out. They are in normal state (i.e., NS), the series arc fault occurred at the front of the inverter (i.e., SAFOFI), and the series arc fault occurred at the back of the inverter (i.e., SAFOBI), respectively. In NS state, there is no series arc fault generator in the circuit. In SAFOFI state, a series arc fault generator was connected in series at the position of F1 in the A-phase circuit. In SAFOBI state, a series arc fault generator was connected in series at the position of F2 in the A-phase circuit. Here, the A-phase is called fault phase. A HAS14Z type current transformer was used to measure the fault phase current signal. It was installed at the front of the inverter in the A-phase circuit. The measured current signal was transmitted to a computer by a data acquisition card, and was displayed and stored in a self-developed application program. The application program was developed by using a Labview software. The sampling frequency of the signal is 10 kHz.

The series arc fault generator is shown in Fig. 2. A flat-headed carbon rod and a pointed copper rod were used as the stationary and movable electrode, respectively. The contact and separation

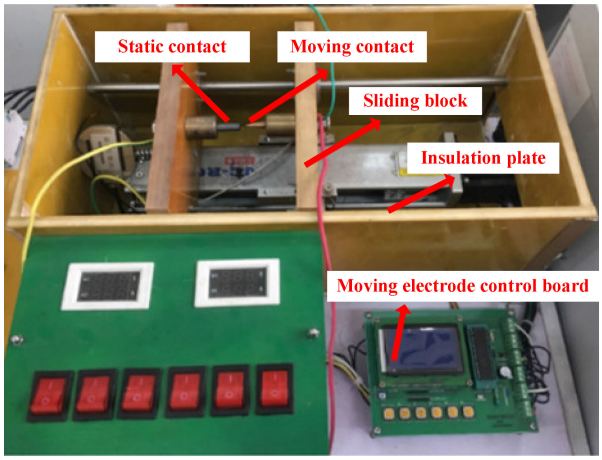

Fig. 2. Series arc fault generator.

TABLE I
EXPERIMENTAL SCHEME

Group No.	Experimental power supply	Working condition
1-6	U1, U2, U3, U4, U5, U6	NS
7-12	U1, U2, U3, U4, U5, U6	SAFOFI
13-18	U1, U2, U3, U4, U5, U6	SAFOBI

TABLE II
HARMONIC PARAMETERS OF U3-U6 POWER SUPPLY

Number of harmonics	Harmonic contents and phase angle			
	U3	U4	U5	U6
3	1.1%/0°	2.2%/0°	4.9%/0°	3.0%/180°
5	2.8%/0°	5.6%/0°	1.6%/0°	2.75%/0°
7	1.4%/0°	2.8%/0°	2.7%/0°	2.40%/180°
9	2.3%/0°	4.6%/0°	0.0%/0°	2.0%/0°
11	1.5%/0°	3.0%/0°	1.4%/0°	1.4%/180°
13	0.0%/0°	0.0%/0°	0.0%/0°	0.8%/0°
15	0.0%/0°	1.4%/0°	2.0%/0°	0.0%/0°
17	0.0%/0°	0.0%/0°	1.1%/0°	0.0%/0°
21	0.0%/0°	1.0%/0°	0.0%/0°	0.0%/0°

of the two electrodes were achieved by controlling a stepper motor. Then, an arc fault occurs during the contact and separation of the two electrodes.

B. Experimental Scheme

The experimental scheme is shown in Table I. There are 18 groups of experiments. The experimental current is 12 A. Six kinds of power supplies were used. In Table I, U1 is a commercial power supply, U2–U6 are programmable power supplies. Where U2 is an ideal three-phase power supply with standard sinusoidal wave. U3-U6 are three-phase power supplies with different harmonic contents and phase angle, as shown in Table II.

C. Analysis of Experimental Results

The measured current waveforms are shown in Fig. 3. The inverter is a non-linear load. In normal state, the CSMFI is shown in Fig. 3(a). When the power supply is U2, the CSMFI presents double-peak characteristics. When the power supply is U3-U6, the CSMFI appears burr and distortion. Especially in the case of U4 and U6, the waveforms of the CSMFI become very

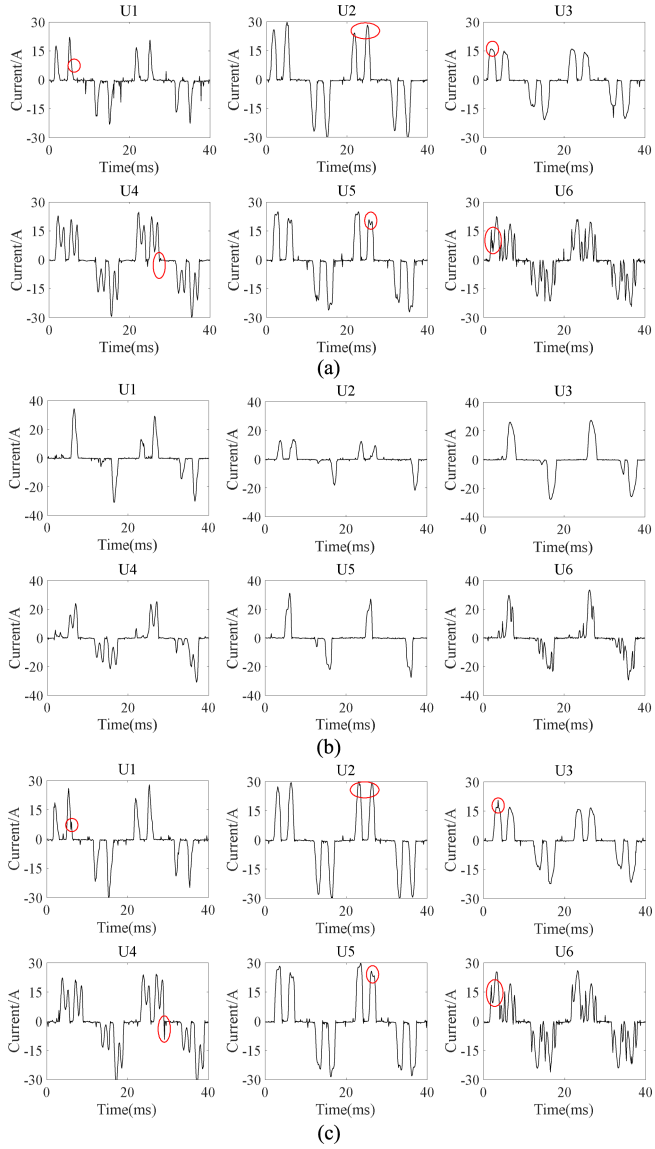

Fig. 3. Waveforms of the CSMFI. (a) NS. (b) SAFOFI. (c) SAFOBI.

complex. The increased burrs and high-frequency components are similar to the fault features of the series arc fault, which makes it difficult to extract the fault features. When a series arc fault occurred at the front of the inverter, the CSMFI has very obvious changes. It changes from double peaks to single peak, as shown in Fig. 3(b). When a series arc fault occurred at the back of the inverter, the CSMFI also has some changes. It changes the amplitude difference of the double peaks and appears burrs in some positions, as shown in Fig. 3(c). Compared with the case, a series arc fault occurred at the front of the inverter, the degree of waveform variation is much smaller in this case. Some waveform features of the CSMFI were marked with red circles in Fig. 3(a) and (c).

As shown in Fig. 3, no matter the series arc fault occurs at the front or back of the inverter, it will have a certain impact on the CSMFI. The fault features of the series arc fault can be extracted by analyzing the CSFMI. However, when the series

arc fault occurs at the back of the inverter, the fault features included in the current waveform are much weaker. It is difficult to effectively detect the series arc fault occurred at the back of the inverter only by analyzing the time domain characteristics of the CSMFI. So the further in-depth analysis of the CSMFI is needed to obtain the fault features, and then realize the detection of the series arc fault.

III. Fault Feature Extraction

The SVD has important applications in feature extraction field [4], [18], [19], [28]. However, for a one-dimensional (1-D) time series, it is necessary to establish a feature matrix first. The commonly used methods include RATM [18], wavelet transform [4], S-transform [19], and variational mode decomposition (VMD) [28], etc. On the basis of wavelet analysis and empirical mode decomposition, EWT was proposed by Gilles in 2013 [29]. It is a new time-frequency analysis method with the advantages of non-modal aliasing and smaller calculation amount. EWT is a widely used signal feature extraction method. But it was seldom applied in the detection of the ac series arc fault.

To better extract the fault features of the series arc fault, EWT was first used to decompose the CSMFI into different frequency bands. It can avoid the high-frequency features of the series arc fault being drowned by the high-energy power frequency components. Then, a RATM was established for each decomposed signal. Next, the singular values of each RATM were calculated and selected. The selected singular values were used as the fault features. The method has the following advantages.

a) It can extract a large number of fault features from each decomposed signal by utilizing the excellent feature extraction ability of SVD.
b) By selecting the singular values, the SVD filter is implemented strictly, which makes the method have strong anti-interference ability.

Therefore, the EWT-RATM-SVD algorithm was used to extract the fault features of the series arc fault.

A. Basic Theory

1) EWT: EWT can adaptively divide the Fourier spectrum according to the signal features, and extract the modal components with a set of orthogonal wavelet filters.

According to the Shannon sampling theorem, the Fourier spectrum range of a signal can be set to $[0, \pi]$. The Fourier spectrum is adaptively divided into *N* continuous bands, and each band can be expressed as follows [30], [31]:

$$\Lambda_n = [\omega_{n-1}, \omega_n] n = 1, 2, \cdots, N \tag{1}$$

where ω_{n} is the boundary of the frequency band interval. ω_0=0, ω_{N}=π, and $\omega_1 \sim \omega_{\mathrm{N}-1}$ are the midpoints of the frequency corresponding to the two adjacent minimums in the signal Fourier spectrum.

With each ω_{n} as the center, the interval division is completed. And the corresponding band-pass filter is set for each interval Λ_n by empirical wavelet. The width of the transition band of the band-pass filters is T_{n}=$2\tau_{\mathrm{n}}$.

The construction formulas of the empirical wavelet function and wavelet function are as follows:

$$\hat{\phi}_{\mathrm{n}}(\omega) = \begin{cases} 1; & |\omega| \le (1-\gamma)\omega_n \\ \cos[\frac{\pi}{2}\beta(\frac{1}{2\gamma\omega_n}(|\omega| - (1-\gamma)\omega_n))]; & (1-\gamma)\omega_n \le |\omega| \le (1+\gamma)\omega_n \\ 0; & \text{other} \end{cases} \tag{2}$$

$$\hat{\varphi}_{\mathrm{n}}(\omega) = \begin{cases} 1; & (1+\gamma)\omega_n \le |\omega| \le (1-\gamma)\omega_{n+1} \\ \cos[\frac{\pi}{2}\beta(\frac{1}{2\gamma\omega_{n+1}}(|\omega| - (1-\gamma)\omega_{n+1}))]; & (1-\gamma)\omega_{n+1} \le |\omega| \le (1+\gamma)\omega_{n+1} \\ \sin[\frac{\pi}{2}\beta(\frac{1}{2\gamma\omega_n}(|\omega| - (1-\gamma)\omega_n))]; & (1-\gamma)\omega_n \le |\omega| \le (1+\gamma)\omega_{n+1} \\ 0; & \text{other} \end{cases} \tag{3}$$

$$\beta(\mathrm{x}) = x^4(35 - 84x + 70x^2 - 20x^3) \tag{4}$$

$$\gamma < \min_n \left(\frac{\omega_{n-1} - \omega_n}{\omega_{n+1} + \omega_n} \right). \tag{5}$$

Let $F^{-1}[\,]$ represent the inverse Fourier transform, $W_{\mathrm{i}}(0, \mathrm{t})$ is the approximate coefficient of the inner product operation between the scale function and the signal, and $W_{\mathrm{i}}(n, \mathrm{t})$ is the detail coefficient of the inner product operation between the empirical wavelet function and the signal. Then, the signal $i(t)$ can be reconstructed as follows:

$$\begin{aligned} i(t) &= W_{\mathrm{i}}(0, \mathrm{t}) * \phi_1(t) + \sum_{n=1}^{N} (n, t) * \varphi_n(t) \\ &= F^{-1}[W_{\mathrm{i}}(0, \omega) * \phi_1(\omega) + \sum_{n=1}^{N} (n, \omega) * \varphi_n(\omega)] \end{aligned}. \tag{6}$$

The signal $i(t)$ can be decomposed into several modal components, that is

$$\begin{cases} f_0(t) = W_{\mathrm{i}}(0, \mathrm{t}) * \phi_1(t) \\ f_k(t) = W_{\mathrm{i}}(k, \mathrm{t}) * \varphi_k(t) \end{cases}. \tag{7}$$

2) RATM: The ATM is a common method of architecting a matrix for time series signals. Assuming a 1-D signal is *X*, $X = [x_1, x_2, \cdots x_N]$, then its ATM is

$$A = \begin{bmatrix} x_1 & x_2 & \cdots & x_j \\ x_2 & x_3 & \cdots & x_{j+1} \\ \vdots & \vdots & \vdots & \vdots \\ x_m & x_{m+1} & \cdots & x_{m+j-1} \end{bmatrix}. \tag{8}$$

Conventional ATM is also called Hank matrix. The data of adjacent rows in the matrix differ by only one data point. So the data of adjacent rows are highly correlated, and a large number of data are re-used. In view of the above-mentioned problem, a time delay step *t* can be reasonably introduced, and a new matrix is obtained. The matrix is called RATM, whose expression is

$$A = \begin{bmatrix} x_1 & x_2 & \cdots & x_j \\ x_{1+t} & x_{2+t} & \cdots & x_{j+t} \\ \vdots & \vdots & \vdots & \vdots \\ x_{1+(m-1)t} & x_{2+(m-1)t} & \cdots & x_{j+(m-1)t} \end{bmatrix}. \tag{9}$$

3) SVD: The SVD is an orthogonal matrix decomposition method. For a matrix $A_{\mathrm{m*n}}$, there must exist two unitary matrices $\mathbf{U}_{m*m}$ and $\mathbf{V}_{n*n}$, and a diagonal matrix Σ_{m*n}, to satisfy the equation $A = \mathbf{U}\Sigma\mathbf{V}^T$. Where $\Sigma_{m*n} =$

$dig(\lambda_1, \lambda_2 \ldots, \lambda_r, 0, \ldots, 0), \lambda_1, \lambda_2 \ldots, \lambda_r$ are the singular values of the matrix $A_{\mathrm{m*n}}$. Singular value has good stability, and it contains important information in the matrix. Moreover, the important information is directly related to the magnitude of the singular value. So the SVD was widely used in the field of feature extraction and fault diagnosis [19].

B. Research on EWT-RATM-SVD Algorithm

In order to better extract the fault features of the series arc fault in the CSMFI, a new feature extraction method based on EWT-RATM-SVD was proposed. The implementation steps are as follows.

1) *Signal decomposition:* The current signal of two cycles was extracted. As the frequency of the current signal is 50 Hz, and its sampling frequency is 10 kHz, so there are 400 sample data for two cycles of the signal. In order to eliminate the effect of current amplitude on signal analysis, the RMS of the current signal was used to normalize the CSMFI. The CSMFI was decomposed by EWT. By analyzing the decomposition results of different layers, it is finally determined that the current signal needs to be decomposed into five layers.
2) *Construction of the RATM:* Five modal components were obtained by conducting EWT decomposition on the CSMFI. And the corresponding RATM for each modal component was constructed. So there are five RATMs. In order to ensure that the data is not re-used and lost, and obtain a square matrix, the time delay step *t* is set to 20. And the number of rows and columns of the RATM are also set to 20.
3) *Establishment of the fault feature vector:* The SVD was performed on the five RATMs, and twenty singular values were obtained for each matrix. In order to filter the interference signal, the first two singular values of each RATM were selected to establish the fault feature vector of the series arc fault.

C. Fault Features Analysis of the Series Arc Fault

The EWT decomposition results of the CSMFI under U3 and U6 power supply conditions are shown in Fig. 4. It shows that all the modal components have certain changes when a series arc fault occurs. When the series arc fault occurs at the back of the inverter, the fault features included in these modal components are more obvious than that in the original CSMFI signal.

The fault features of the series arc fault extracted by the EWT-RATM-SVD method are shown in Fig. 5. The change of fault features is very obvious when the series arc fault occurs at the front of the inverter. While the change of the fault features of the series arc fault occurred at the back of the inverter is less obvious.

IV. Performance Analysis of the Proposed Algorithm

A. Identification Results of the Series Arc Fault

In order to test the effectiveness of the fault features extracted by the EWT-RATM-SVD algorithm, a large number of identification tests of the series arc fault were conducted by using an

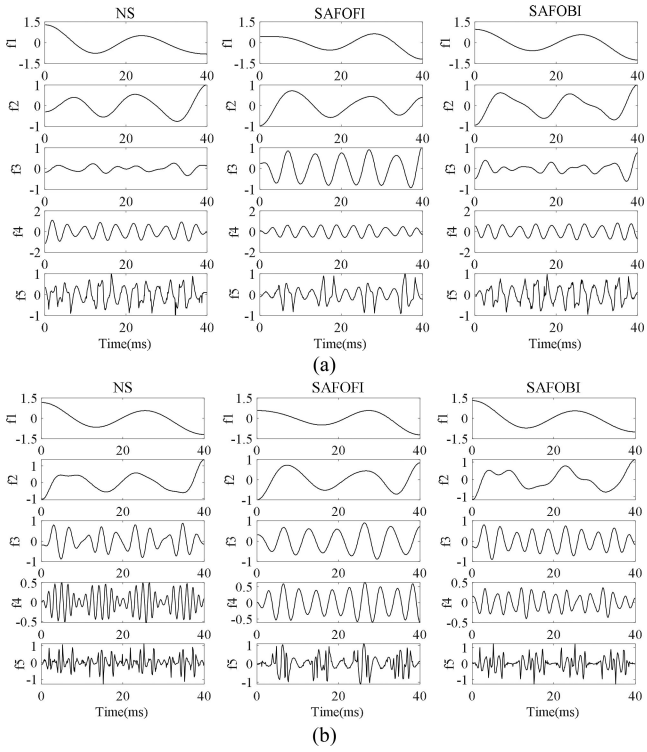

Fig. 4. EWT decomposition results of CSMFI under different power supply conditions. (a) Under U3 power supply conditions. (b) Under U6 power supply conditions.

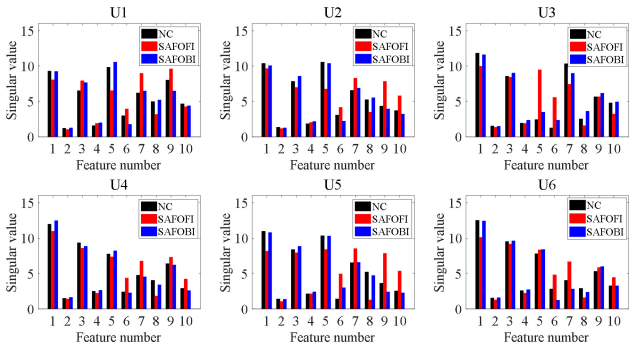

Fig. 5. Fault features of the series arc fault.

SVM. The penalty parameter *c* and the kernel function parameter *g* of the SVM are important, because they will directly affect the identification results. So they are optimized by using the grid search and particle swarm optimization (GS-PSO) algorithm. The detailed optimization principle and calculation process can refer to [32].

In Section II-B, a total of eighteen groups of experiments were carried out, as shown in Table I. For each group of experiment, 200 segments of current data were intercepted. The length of each data segment is two current cycles. The EWT-RATM-SVM algorithm was used to calculate the fault features of each data segment. So there are 3600 fault feature samples in total, which corresponding to 3600 data segments. The category label of the sample in normal state is set to 0, while the category label in series arc fault state is set to 1. All the 3600 samples were equally

divided into training samples and testing samples. Then, one-fifth of the training samples were taken and used to optimize the parameters of the SVM.

The SVM was optimized by using the GS-PSO algorithm. The obtained optimal parameters c and g are 25.1 and 5.0, respectively.

An SVM identification model of the series arc fault was established with the training samples and the optimal parameters c and g. The identification tests were carried out by inputting the testing samples into the SVM identification model. It shows that the identification accuracy of the series arc fault is 99.67%. The false detection rate is 0.11%. The missing detection rate of the series arc fault occurred at the front and back of the inverter is 0.06% and 0.16%, respectively. Here, the false detection rate refers to the ratio of the number of samples judged as arc fault state in normal state to the total number of testing samples. The missing detection rate refers to the ratio of the number of samples judged as normal state in arc fault state to the total number of testing samples.

B. Comparison of Different Fault Feature Extraction Methods

In order to verify the superiority of the proposed method, the following feature extraction methods were compared and analyzed.

1) *Reference [23]:* Two current signals and a voltage signal were used to extract the fault features. The kernel principal component analysis (KPCA) was first conducted on these signals. And then the kurtosis and skewness of the fifth and sixth principal components of the KPCA were extracted as the fault features.
2) *Reference [19]:* The S-transform of the CSMFI was carried out, and an amplitude matrix was established. The singular values of the matrix were calculated. Then the obtained low-dimensional singular values were used as the fault features.
3) *Reference [4]:* The wavelet transform of the CSMFI was carried out, and a Hank matrix was constructed by using the obtained wavelet coefficients. The SVD was performed to the matrix, and the singular values were obtained. Then the average value, RMS, and standard deviation of these singular values were used as the fault features.
4) *Reference [2]:* The CZT of the CSMFI was carried out, and the spectrums from 0 to 500 Hz were obtained. The following variables were calculated and used as the fault features. They are the average value of the low-frequency spectrum difference of two-segment currents, the change rate of the second, fourth, sixth harmonic, the average value of the frequency spectrum, and the average value of the current signal difference, respectively.
5) *Reference [5]:* The three-layer wavelet decomposition of the CSMFI was conducted with DB10 wavelet basis, and the energies of the high-frequency components were used as the fault features.
6) *Reference [28]:* The VMD of the CSMFI was conducted, and several modal components were obtained. A matrix was constructed by using these modal components. The singular values of the matrix were used as the fault features.
7) *EWT-SVD:* The five-layer EWT of the CSMFI was conducted. A matrix was constructed by using the obtained modal components. And the singular values of the matrix were used as the fault features.
8) *RATM-SVD:* A RATM was constructed by using the CSMFI. And the singular values of the matrix were used as the fault features.

TABLE III
ACCURACY AND OPERATION TIME OF THE SERIES FAULT DETECTION WITH DIFFERENT FEATURE EXTRACTION METHODS

Method No.	feature extraction method	A1 /%	A2 /%	A3 /%	operation time /ms
1	Reference [23]	96	94.7	94.2	1543
2	Reference [19]	78.7	70.8	71.8	1.6
3	Reference [4]	85.4	86.8	82.3	9.2
4	Reference [2]	76.3	85.5	64.6	0.72
5	Reference [5]	85.2	86.1	80.6	1.9
6	Reference [28]	95.9	96.8	94.1	43.8
7	EWT-SVD	95.3	94.0	95.0	0.6
8	RATM-SVD	94.3	95.3	92.3	0.09
9	Proposed method	99.7	99.8	99.6	0.68

The fault features of the series arc fault were calculated by using the above-mentioned eight methods. The calculation was conducted by using MATLAB software installed in a computer. The main frequency of the computer is 2.9 GHz. For each method, the operation time of extracting fault features was calculated.

There are eighteen groups of experiments in Table I. For each measured current signal, 100 segments of current data were intercepted, and the corresponding fault features were calculated by using the EWT-RATM-SVD algorithm. So there are 1800 sets of fault features in total, which were used as training samples. An identification model of the series arc fault was established with the GS-PSO optimized SVM.

The identification results of the series arc fault were tested in the following three cases.

Case 1: For each measured current signal in all groups of the experiment in Table I, 100 fault features were calculated and used as the testing samples. The identification accuracy, in this case, is labeled as *A1*.

Case 2: For each measured current signal in the first twelfth groups of the experiment in Table I, 100 fault features were calculated and used as the testing samples. They were used to test the identification accuracy of the series arc fault occurred at the front of the inverter. The corresponding identification accuracy is labeled as *A2*.

Case 3: For each measured current signal in the 1st–6th group, and the 13th –18th group of the experiment in Table I, 100 fault features were calculated and used as the testing samples. They were used to test the identification accuracy of the series arc fault occurred at the back of the inverter. The corresponding identification accuracy is labeled as *A3*.

The test results of the above-mentioned three cases are shown in Table III. And the following conclusions can be obtained.

1) As for the first five fault feature extraction methods, which were proposed in References [23], [19], [4], [2], and [5],

TABLE IV
IDENTIFICATION RESULTS OF THE SERIES ARC FAULT UNDER DIFFERENT LEVELS OF GAUSS NOISE CONDITIONS

signal-to-noise ratio of the Gauss noise	A1/%	A2/%	A3/%
25dB	99.7	99.8	99.6
20dB	99.5	99.5	99.3
15 dB	98.7	99.1	98.2
10dB	90.5	90.7	85.8

the identification accuracy of the series arc fault occurred at the back of the inverter is lower than 95%. The operation time of the proposed method is the shortest.

2) As for the 6th and 7th fault feature extraction methods, there is little difference in the identification accuracy of the series arc fault. It indicates that the decomposition performance of the VMD and the EWT algorithm is no obvious difference under the experimental conditions in this article. Since the calculation amount of the EWT is much smaller than that of the VMD, the EWT algorithm has more advantages from the perspective of real-time performance.
3) Compared with the 7th and 8th fault feature extraction methods, the operation time of the proposed method is longer due to the combined calculations of the EWT and the RATM. But the total operation time of the method is still less than 1 ms. Moreover, the proposed method has the highest identification accuracy. It also shows that the operation of the EWT and the RATM in the EWT-RATM-SVD algorithm is very necessary.

C. Anti-Interference Ability Test

In order to test the anti-interference ability of the proposed method, the Gaussian noise with different signal-to-noise ratio of 25 dB, 20 dB, 15 dB, and 10 dB was first added to the CSMFI. The fault features of the series arc fault were extracted by using the EWT-RATM-SVD algorithm, and then the identification accuracy of the series arc fault under different levels of Gauss noise conditions were tested by using the SVM recognition model established in Section IV-A. The test results are shown in Table IV. If the signal-to-noise ratio of the Gaussian noise is not lower than 15 dB, the noise will have little influence on the identification accuracy of the proposed method. When the series arc fault occurs at the back of the inverter, since the fault features included in the CSMFI are weak, the Gauss noise has a greater impact on the identification accuracy.

V. APPLICABILITY OF THE PROPOSED ALGORITHM UNDER DIFFERENT EXPERIMENTAL CONDITIONS

A. Applicability Test in the Three-Phase Motor Load Circuit

In order to test the applicability of the EWT-RATM-SVD algorithm in other load circuits, another series arc fault experiments were carried out in a three-phase motor load circuit. The experimental scheme is shown in Table V.

The method stated in Section IV-A was used to test the identification accuracy of the series arc fault. The identification accuracy of the series arc fault occurred in the three-phase motor load circuit is 98.2%. Where the false detection rate is 1.8%, and the missing detection rate is 0%. It shows that the proposed method is also applicable to identify the series arc fault occurred in the three-phase motor load circuit.

TABLE V
EXPERIMENTAL SCHEME FOR THE SERIES ARC FAULT EXPERIMENTS IN A THREE-PHASE MOTOR LOAD CIRCUIT

Group No.	Experimental power supply	Working condition
1-3	U1, U5, U6	Normal state
4-6	U1, U5, U6	Arc fault state

TABLE VI
EXPERIMENTAL SCHEME OF THE SERIES ARC FAULT EXPERIMENTS UNDER DIFFERENT INVERTER'S OPERATION PARAMETERS CONDITIONS

Group No.	Experimental power supply	Working condition	Working Frequency	PWM Carrier Frequency
1-3	U1, U5, U6	NS	40Hz	8kHz
4-6	U1, U5, U6	SAFOFI	40Hz	8kHz
7-9	U1, U5, U6	SAFOBI	40Hz	8kHz
10-12	U1, U5, U6	NS	45Hz	8kHz
13-15	U1, U5, U6	SAFOFI	45Hz	8kHz
16-18	U1, U5, U6	SAFOBI	45Hz	8kHz
19-21	U1, U5, U6	NS	50Hz	3kHz
22-24	U1, U5, U6	SAFOFI	50Hz	3kHz
25-27	U1, U5, U6	SAFOBI	50Hz	3kHz
28-30	U1, U5, U6	NS	50Hz	13kHz
31-33	U1, U5, U6	SAFOFI	50Hz	13kHz
34-36	U1, U5, U6	SAFOBI	50Hz	13kHz

TABLE VII
IDENTIFICATION RESULTS OF THE SERIES ARC FAULT UNDER DIFFERENT INVERTER'S OPERATION PARAMETERS CONDITIONS

Working frequency	PWM carrier frequency	Identification accuracy/ %
40Hz	8kHz	97.6
45Hz	8kHz	97.9
50Hz	3kHz	99.6
50Hz	13kHz	96.3

B. Applicability Test Under Different Inverter's Operation Parameters Conditions

For the series arc fault stated in Section II-B, the working frequency of the inverter is 50 Hz, and the PWM carrier frequency of the inverter is 8 kHz. In order to test the applicability of the proposed method under different inverter's operation parameters conditions, the series arc fault experiments were added. The experimental current is 12 A. The detailed experimental scheme is shown in Table VI.

The method stated in Section IV-A was used to test the identification accuracy of the series arc fault. The test results are shown in Table VII. It shows that the identification accuracy is higher than 95%. It means that the proposed method is also valid when the working frequency or PWM carrier frequency of the inverter varies.

C. Applicability Test Under Different Working Current Conditions

In order to verify the applicability of the proposed method at different working current of the circuit, the series arc fault experiments under different working current conditions were added. The working current was set to 14 A by adjusting the

TABLE VIII
EXPERIMENTAL SCHEME OF THE SERIES ARC FAULT EXPERIMENTS UNDER DIFFERENT WORKING CURRENT CONDITIONS

Group No.	Experimental power supply	Working condition
1-3	U1, U5, U6	NS
4-6	U1, U5, U6	SAFOFI
7-9	U1, U5, U6	SAFOBI

TABLE IX
EXPERIMENTAL SCHEME OF THE TRANSIENT SERIES ARC FAULT EXPERIMENTS

Group No.	Experimental power supply	Working condition	Number of repetitions for each experiment
1-3	U1, U5, U6	NS	200
4-6	U1, U5, U6	From NS to SAFOFI	200
7-9	U1, U5, U6	From NS to SAFOBI	200

friction load in Fig. 1. The detailed experimental scheme is shown in Table VIII.

The identification accuracy of the series arc fault occurred in this case, was tested by using the method stated in Section IV-A. Test results showed that the identification accuracy is 97.6%. It means that the proposed method is still valid under different working current conditions.

D. Applicability Test Under Transient Series Arc Fault Conditions

In order to verify the applicability of the proposed method under transient series arc fault conditions, additional transient arc fault experiments were conducted by using the experimental platform shown in Fig. 1. Here, the transient series arc fault refers to the sudden occurrence of the series arc fault during the normal operation of the circuit. In other words, it is the transition process of the circuit from the normal state to the series arc fault state. The transient series arc fault was generated by controlling the reciprocating movement of the moving contact of the series arc fault generator, which was shown in Fig. 2. The detailed experimental scheme is shown in Table IX.

When the sample data is intercepted by using the CSMFI signal measured in group no. 4–9 in Table IX, it must be ensured that each sample data contains the transient process from the normal state to the series arc fault state. The length of the sample data in this work is 2 current cycles. Therefore, each intercepted sample data is composed of the previous cycle and the next cycle at the moment when the series arc fault occurs.

The identification accuracy of the series arc fault occurred in this case, was tested by using the method stated in Section IV-A. Test results showed that the identification accuracy is 98.9%. It means that the proposed method is still valid under transient series arc fault conditions.

VI. CONCLUSION

Aiming at the problem that there is no related research on the detection method of the series arc fault occurred at the back of the inverter in the three-phase motor with inverter circuit, a new arc feature extraction method of the series arc fault was proposed. The fault features can be extracted from the CSMFI by using the EWT-RATM-SVD algorithm. It can be used to detect the series arc fault occurred at the front and back of the inverter. The following conclusions were obtained.

1) No matter the series arc fault generated at the front or back of the inverter, the CSMFI will contain the fault features of the series arc fault. It is feasible to use the CSMFI to detect the series arc fault occurred in the front and back of the inverter.
2) The proposed EWT-RATM-SVD method can extract effectively the fault features of the series arc fault occurred in the three-phase motor with inverter circuit under complicated harmonic power supply conditions. Even if there is no current transformer installed at the back of the inverter, the series arc fault can also be identified by using the proposed feature extraction method and the GS-PSO optimized SVM.
3) The proposed EWT-RATM-SVD method has strong anti-interference ability. The Gauss noise, whose signal-to-noise ratio is not lower than 15 dB, has little influence on the results of the extracted fault features. Compared with the existing methods, the proposed method has higher identification accuracy and less calculation amount. It can provide a reference for the feature extraction of a signal in the arc fault or other fields.

In this article, the hardware implementation of the proposed method was not discussed. Due to less computation, the method has certain advantages in the microprocessor implementation. In the future, we will continue to carry out the research on the implementation of the method in commercial microprocessors, and develop the corresponding AFCI.

ACKNOWLEDGMENT

The authors would like to thank the reviewers for their many constructive comments.

REFERENCES

[1] T. Yin and R. He, *Low Voltage Electrical Apparatus Technical Manuals*. Beijing, China: China Machine Press, 2014.
[2] G. Artale, A. Cataliott, V. Cosentino, D. Di Cara, S. Nuccio, and G. Tinè, "Arc fault detection method based on CZT low-frequency harmonic current analysis," *IEEE Trans. Instrum. Meas.*, vol. 66, no. 5, pp. 888–896, May 2017.
[3] N. Qu, J. Wang, and J. Liu, "An arc fault detection method based on current amplitude spectrum and sparse representation," *IEEE Trans. Instrum. Meas.*, vol. 68, no. 10, pp. 3785–3792, Oct. 2019.
[4] Q. Lu, T. Wang, Z. Li, and C. Wang, "Detection method of series arcing fault based on wavelet transform and singular value decomposition," *Trans. China Electrotech. Soc.*, vol. 32, no. 17, pp. 208–217, 2017.
[5] C. Wu and Y. Liu, "Smart detection technology of serial arc fault on low-voltage indoor power lines," *Int. J. Elect. Power Energy Syst.*, vol. 69, pp. 391–398, 2015.
[6] Y. Wang, L. Hou, K. C. Paul, Y. Ban, C. Chen, and T. Zhao, "ArcNet: Series AC arc fault detection based on raw current and convolutional neural network," *IEEE Trans. Ind. Informat.*, vol. 18, no. 1, pp. 77–86, Jan. 2022.
[7] J. C. Kim, D. O. Neacşu, R. Ball, and B. Lehman, "Clearing series AC arc faults and avoiding false alarms using only voltage waveforms," *IEEE Trans. Power Del.*, vol. 35, no. 2, pp. 946–956, Apr. 2020.
[8] J. Jiang, W. Li, Z. Wen, Y. Bie, H. Schwarz, and C. Zhang, "Series arc fault detection based on random forest and deep neural network," *IEEE Sensors J.*, vol. 21, no. 15, pp. 17171–17179, Aug. 2021.
[9] K. Zeng, L. Xing, Y. Zhang, and L. Wang, "Characteristics analysis of AC arc fault in time and frequency domain," in *Proc. Prognostics Syst. Health Manage. Conf.*, 2017, pp. 1–5.

[10] B. Cui and D. Tong, "Aviation AC series arc fault detection based on Levene test," *Trans. China Electrotech. Soc.*, vol. 36, no. 14, pp. 3034–3042, 2021.

[11] F. Gao *et al.*, "Identification of AC aviation arc fault based on ensemble empirical mode decomposition," *Adv. Technol. Elect. Eng. Energy*, vol. 39, no. 4, pp. 73–80, 2020.

[12] B. Cui, D. Tong, and Z. Li, "Aviation arc fault detection based on generalized S transform," *Proc. CSEE*, vol. 41, no. 23, pp. 8241–8250, 2021.

[13] P. Parikh, D. Allcock, R. Luna, and J. Vico, "A novel approach for arc-flash detection and mitigation: At the speed of light and sound," *IEEE Trans. Ind. Appl.*, vol. 50, no. 2, pp. 1496–1502, Mar./Apr. 2014.

[14] G. A. Hussain, M. Shafiq, M. Lehtonen, and M. Hashmi, "Online condition monitoring of MV switchgear using D-Dot sensor to predict arc-faults," *IEEE Sensors J.*, vol. 15, no. 12, pp. 7262–7272, Dec. 2015.

[15] J. Wang, W. Lin, Z. Wang, J. Li, W. He, and P. Wang, "Online detecting device for switchgear arc based on ultraviolet detection," *Power Syst. Protect. Control*, vol. 39, no. 5, pp. 128–133, 2011.

[16] J. Zhang and H. Ma, "Online monitoring and protection system for the arc fault of the mining high-voltage switchgear," *Power Syst. Protect. Control*, vol. 41, no. 11, pp. 141–145, 2013.

[17] S. A. Saleh, A. S. Aljankawey, R. Errouissi, and M. A. Rahman, "Phase-based digital protection for arc flash faults," *IEEE Trans. Ind. Appl.*, vol. 52, no. 3, pp. 2110–2121, May/Jun. 2016.

[18] H. Gao *et al.*, "Research on feature of series arc fault based on improved SVD," in *Proc. IEEE Holm Conf. Elect.*, 2017, pp. 325–331.

[19] F. Guo, H. Gao, Z. Wang, J. You, Y. Deng, and C. Chen, "Feature extraction method of series arc fault based on ST-SVD-PCA," *J. China Coal Soc.*, vol. 43, no. 3, pp. 888–896, 2018.

[20] F. Guo, Y. Deng, Z. Wang, J. You, and H. Gao, "Series arc fault characteristics based on gray level-gradient co-occurrence matrix," *Trans. China Electrotech. Soc.*, vol. 33, no. 1, pp. 71–81, 2018.

[21] W. Li, Y. Liu, Y. Li, and F. Guo, "Series arc fault diagnosis and line selection method based on recurrent neural network," *IEEE Access*, vol. 8, pp. 177815–177822, 2020.

[22] H. Gao, Z. Wang, A. Tang, C. Han, F. Guo, and B. Li, "Research on series arc fault detection and phase selection feature extraction method," *IEEE Trans. Instrum. Meas.*, vol. 70, no. 5, May 2021, Art. no. 2004508.

[23] C. Han, Z. Wang, A. Tang, H. Gao, and F. Guo, "Recognition method of AC series arc fault characteristics under complicated harmonic conditions," *IEEE Trans. Instrum. Meas.*, vol. 70, no. 1, Jan. 2021, Art. no. 3509709.

[24] H. P. Park, M. Kim, J. H. Jung, and S. Chae, "Series DC arc fault detection method for PV systems employing differential power processing structure," *IEEE Trans. Power Electron.*, vol. 36, no. 9, pp. 9787–9795, Sep. 2021.

[25] W. Miao, Q. Xu, K. H. Lam, P. W. T. Pong, and H. V. Poor, "DC arc-fault detection based on empirical mode decomposition of arc signatures and support vector machine," *IEEE Sensors J.*, vol. 21, no. 5, pp. 7024–7033, Mar. 2021.

[26] S. Chen, X. Li, and J. Xiong, "Series arc fault identification for photovoltaic system based on time-domain and time-frequency-domain analysis," *IEEE J. Photovolt.*, vol. 7, no. 4, pp. 1105–1114, Jul. 2017.

[27] W. Gao and R. J. Wai, "Series arc fault detection of grid-connected PV system via SVD denoising and IEWT-TWSVM," *IEEE J. Photovolt.*, vol. 11, no. 6, pp. 1493–1510, Nov. 2021.

[28] Z. Jiang, D. Wei, J. Zhang, and Z. W. Mao, "A study on valve clearance anomaly feature extraction of diesel engines based on VMD and SVD," *J. Vib. Shock*, vol. 39, no. 16, pp. 23–30, 2020.

[29] J. Gilles, "Empirical wavelet transform," *IEEE Trans. Signal Process.*, vol. 61, no. 16, pp. 3999–4010, Aug. 2013.

[30] T. Siddharth, P. Gajbhiye, R. K. Tripathy, and R. B. Pachori, "EEG-based detection of focal seizure area using FBSE-EWT rhythm and SAE-SVM network," *IEEE Sensors J.*, vol. 20, no. 19, pp. 11421–11428, Oct. 2020.

[31] Y. Xu, S. Fan, C. Tan, and M. Lu, "Power quality disturbance detection and classification in high permeability active distribution network with improved EWT-CMPE," *Power Syst. Technol.*, vol. 44, no. 10, pp. 3991–4000, 2020.

[32] F. Guo, H. Gao, Z. Wang, J. You, A. Tang, and Y. Zhang, "Detection and line selection of series arc fault in multi-load circuit," *IEEE Trans. Plasma Sci.*, vol. 47, no. 11, pp. 5089–5098, Nov. 2019.

Hongxin Gao (Member, IEEE) received the B.S., M.S., and Ph.D. degrees in electrical engineering from Liaoning Technical University, Huludao, China, in 2013, 2015, and 2019, respectively.

He is currently a Lecturer with Liaoning Technical University. His current research interests include electrical contact, electric arc, and intelligent electrical apparatus.

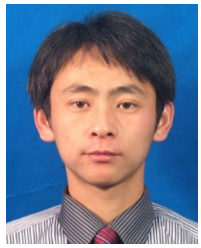

Zhiyong Wang (Member, IEEE) received the B.S. and M.S. degrees in electrical engineering and the Ph.D. degree in safety management engineering from Liaoning Technical University, Huludao, China, in 2005, 2008, and 2017, respectively.

He is currently an Associate Professor with Liaoning Technical University. His research interests include electrical contact, electric arc, and intelligent electrical apparatus.

Congxin Han received the B.S. and M.S. degrees in electrical engineering in 2017 and 2021, respectively, from Liaoning Technical University, Liaoning, China, where he is currently working toward the Ph.D. degree in electrical engineering.

His research interests include electrical contact theory and electric arc.

Aixia Tang received the B.S. degree in electrical engineering from Yanshan University, Qinhuangdao, China, in 2008, and the M.S. degree in electrical engineering in 2011 from Liaoning Technical University, Huludao, China, where she is currently working toward the Ph.D. degree in electrical engineering.

Her current research interests include electrical contact and electric arc.

Fengyi Guo (Senior Member, IEEE) received the B.S. and M.S. degrees in electrical engineering from Fuxin Mining Institute, Fuxin, China, in 1987 and 1990, respectively, and the Ph.D. degree in electrical engineering from Xi'an Jiaotong University, Xi'an, China, in 1997.

He is currently a Professor with the College of Electrical and Electric Engineering, Wenzhou University, Wenzhou, China. He was a Visiting Professor with the University of Pretoria, South Africa and the University of Oxford, U.K., in 2002–2003 and 2008–2009, respectively. He has authored more than 150 articles. His current research interests include electrical contact, electric arc, and intelligent electrical apparatus.

Baifu Li is currently working toward the B.S. degree in electrical engineering with Liaoning Technical University, Huludao, China.

His current research interest is electric arc.